Rad-Pro

User Manual

Version 1.1

Bong Jae Lee, Ph.D. Candidate

Zhuomin Zhang, Associate Professor

George W. Woodruff School of Mechanical Engineering

Georgia Institute of Technology, Atlanta, Georgia 30332.

September 19, 2005

Summary

In order to achieve high-accuracy temperature measurements in rapid thermal processing (RTP) using lightpipe radiation thermometry, it is critical to be able to determine the radiative properties of silicon wafers with thin-film coatings such as silicon dioxide, silicon nitride, and polysilicon. A software tool, **Rad-Pro** (named after **Rad**iative **Pro**perties), has been developed for easy calculation and plotting of the absorptance, emittance, reflectance, and transmittance of silicon wafers in the RTP environments. The calculated results have been verified by comparison with high-accurate spectral reflectance measurements at room temperature. This document explains the theory, formulation, capability, and how to use **Rad-Pro**. Users are welcome to provide feedback for further improvement and upgrade.

Table of Contents

Summary 1

Table of Contents 2

1. Introduction 3

2. Modeling the Radiative Properties of Multilayers 5

- **Coherent Formulation** 5
- **Incoherent Formulation** 7

3. Optical Constants of Silicon and Related Materials 9

- **Empirical Models for the Optical Constants of Lightly Doped Silicon** 9
- **The Drude Model for the Optical Constants of Doped Silicon** 15
- **Other Materials** 20
- **Comparison with Room Temperature Reflectance Measurements** 21

4. Getting Started 23

- **Installation of Files** 23
- **Input Parameters** 24
- **Calculation and Plotting** 34
- **Saving Data** 34

5. Proposed Future Enhancements 37

Acknowledgments 38

References 38

1. Introduction

Rapid thermal processing (RTP) has become a key technology for semiconductor device manufacturing in a variety of applications, such as thermal oxidation, annealing, and thin-film growth. Temperature measurements and control are critically important for continuous improvement of RTP [1,2]. Since the heating source is at a much higher temperature than that of the silicon wafer, radiative energy exchange is the dominant mode of heat transfer. Hence, understanding the radiative properties of silicon and other relevant materials is essential for the analysis of the thermal transport processes. Furthermore, since many RTP furnaces use non-contact lightpipe thermometers, accurate determination of the wafer emittance is necessary for correlating the radiance temperature to the true wafer temperature [3,4].

Earlier, Hebb and coworkers [5] developed a PC-based software package called *Multi-Rad*, which allows the calculation of radiative properties of silicon wafers with thin-film coatings in the wavelength, temperature, and dopant concentration ranges relevant to RTP. However, the validation relied mainly on the comparison with preexisting experimental data. Consequently, its accuracy is inevitably limited to the wavelength, temperature, and dopant concentration ranges of available studies, which are not quite consistent and accurate. In addition, certain parameters used in the Drude model, such as carrier scattering times and carrier concentrations, do not agree with the well-established theory and values. Furthermore, *Multi-Rad* is not easily accessible. For instance, entering of the input parameters needs to follow some tiresome steps, data manipulation in the program is not allowed, and the output is limited to the third decimal point. The radiative properties calculated by *Multi-Rad* are given in terms of an integration of the spectral radiative properties over a wavelength interval $\Delta\lambda$, which is determined by user's input of the wavelength increment. To correctly implement the spectral averaging, however, the wavelength interval $\Delta\lambda$

must be determined based on the considered wavelength region and sample conditions along with other factors [6].

Georgia Institute of Technology and National Institute of Standards and Technology (NIST) have collaborated to develop a reliable and easily accessible software tool, which can predict the radiative properties of silicon wafers in the RTP environments. As the first step towards a fully validated software program, the calculated results have been carefully examined by comparison with the accurate measurements at room temperature using standard facilities in NIST [7]. This software tool, named as **Rad-Pro** (for **Rad**iative **Pro**perties), will allow users to predict the directional, spectral, and temperature dependence of the radiative properties for the multilayer structures consisting of silicon and related materials such as silicon dioxide, silicon nitride, and polysilicon. In **Rad-Pro**, users can choose to use the formulation for coherent, incoherent, and opaque substrate without spectral integration.

Rad-Pro has some unique advantages. First, since it is developed using Excel programming with Visual Basic for Applications (VBA), the manipulation of the data and plots can be done by the same way in Excel with which most of users are already familiar. Second, it allows users to choose the calculation method (i.e. coherent or incoherent formulation) as well as other options, such as the polarization status of incident radiation and an opaque option that treats the silicon substrate as a semi-infinite medium. Third, it is possible to input the optical constants of user-defined materials. This allows **Rad-Pro** to include new materials and to be used for other applications besides RTP. On the other hand, there is large room for future improvement. For instance, the experimental validation of the model has not been performed over all wavelength, temperature, and dopant concentration ranges of interest. Thus, the current version of **Rad-Pro** serves as a prototype of a more complete product yet to be materialized.

2. Modeling the Radiative Properties of Multilayers

The radiative properties, such as reflectance, transmittance, and emittance of multilayer structures largely depend on the direction and wavelength of incident radiation as well as wafer temperature. They are also affected by thin-film coatings and surface roughness. In **Rad-Pro**, it is assumed that the interfaces of each layer are optically smooth and perfectly parallel. In this section, the detailed descriptions of the two methods about modeling the radiative properties of silicon wafer with thin-film coatings are provided.

Coherent Formulation

When the thickness of each layer is comparable or less than the wavelength of electromagnetic waves, the wave interference effects inside each layer become important to correctly predict the radiative properties of multilayer structure of thin films. The transfer-matrix method provides a convenient way to calculate the radiative properties of multilayer structures of

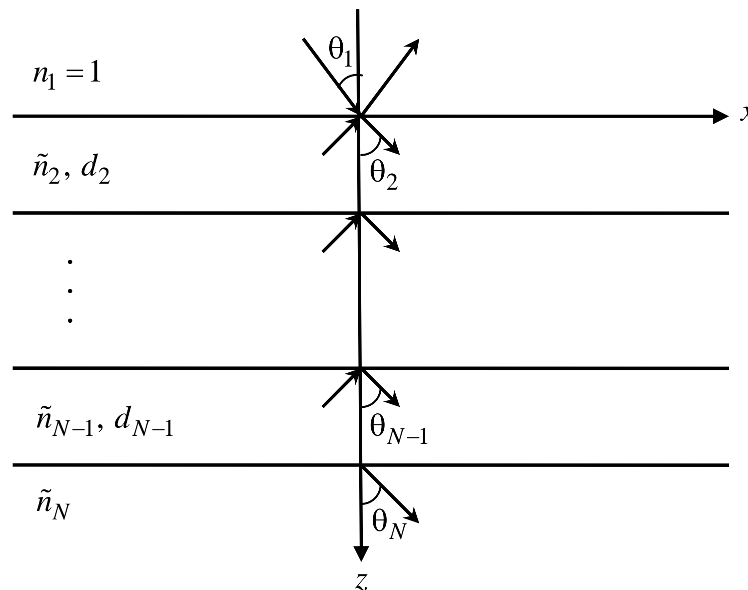

Fig. 1 The geometry for calculating the radiative properties of a multilayer structure

thin films. For the jth medium, the complex refractive index is $\tilde{n}_j = n_j + i\kappa_j$ and the thickness is d_j (see Fig. 1). It is assumed that $\tilde{n}_1 = 1$; that is, the top semi-infinite medium is air. For the calculation, the optical properties of air are assumed to be the same as those of vacuum. The electromagnetic wave is incident from the first medium (air) at an angle of incidence θ_1 and is reflected from or transmitted through the following layers. By assuming that the electric field in the jth medium is a summation of forward and backward waves in the z-direction, the electric field in each layer can be expressed by

$$E_j = \begin{cases} \left[A_1 e^{iq_{1z}z} + B_1 e^{-q_{1z}z} \right] e^{(iq_x x - i\omega t)} & , \ j = 1 \\ \left[A_j e^{iq_{jz}(z-z_{j-1})} + B_j e^{-q_{jz}(z-z_{j-1})} \right] e^{(iq_x x - i\omega t)} & , \ j = 2, 3, \cdots, N \end{cases} \tag{1}$$

where A_j and B_j are the amplitudes of forward and backward waves in the jth layer, respectively, $z_1 = 0$ and $z_j = z_{j-1} + d_j \left(j = 2, 3, .., N-1 \right)$, ω is the angular frequency, and q_x and q_{jz} are parallel and perpendicular components of the wave vector, respectively. Notice that $q_x = \frac{2\pi}{\lambda} n_1 \sin\theta_1$ is conserved throughout the layers, and q_{jz} is given by $q_{jz} = \frac{2\pi}{\lambda} \tilde{n}_j \cos\tilde{\theta}_j$, where λ is the wavelength of the incident radiation in vacuum and $\tilde{\theta}_j = \sin^{-1}(n_1 \sin\theta_1 / \tilde{n}_j)$ is in general complex. By applying boundary conditions at the interfaces, coefficients of A_j and B_j can be related to those of the adjacent layers by a linear equation. Detailed descriptions of how to solve for A_j and B_j can be found in the Refs. [8,9]. Consequently, the radiative properties of the N-layer system are given by

$$\rho = \frac{B_1 B_1^*}{A_1^2} \tag{2a}$$

$$\tau = \frac{\mathrm{Re}(\tilde{n}_N \cos\tilde{\theta}_N)}{n_1 \cos\theta_1} \frac{A_N A_N^*}{A_1^2} \tag{2b}$$

and

$$\varepsilon = 1 - \rho - \tau \tag{2c}$$

where asterisks denote the complex conjugate.

Incoherent Formulation

When the thickness of silicon substrate is much greater than the coherent length, and the considered wavelength falls in the semitransparent region of silicon, interferences in the substrate are generally not observable from the measurements. In this case, the incoherent formulation or geometric optics should be used to predict the radiative properties of the silicon

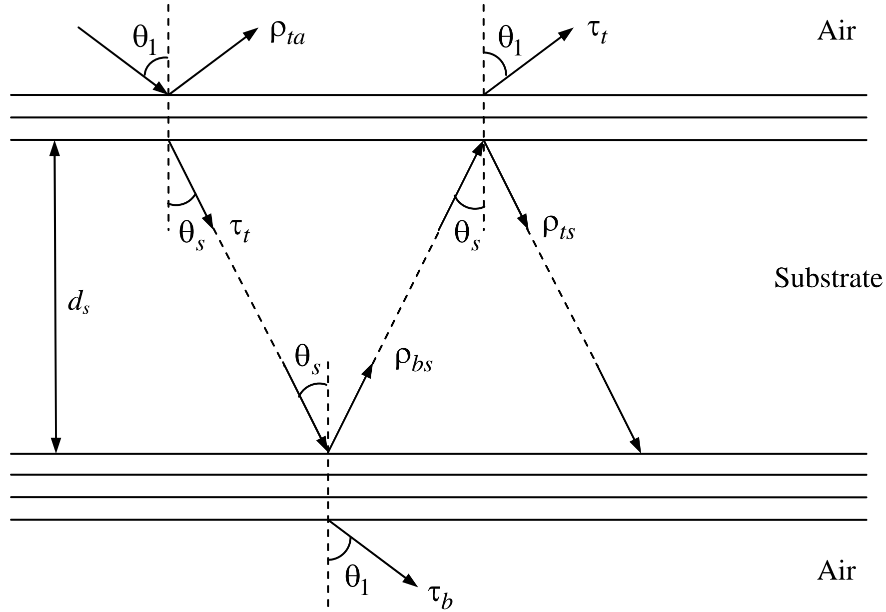

Fig. 2 Schematic of thin-film coatings on both sides of a thick silicon

substrate. Two ways to get around this problem are to use the fringe-averaged radiative properties and to treat thin-film coatings as coherent but the substrate as incoherent [9]. Figure 2 shows the geometry of the silicon wafer with thin-film coatings on both sides. Note that ρ_{ta} and τ_t are the reflectance and transmittance, respectively, of the multilayer structure at the top surface (air−coatings−silicon) for rays incident from air, assuming that the silicon extends to infinite. On the other hand, ρ_{ts} and τ_t are for rays incident from silicon. Note that the transmittance τ_t is the same when absorption inside silicon is negligibly small [10]. Similarly, ρ_{bs} and τ_b are for the multilayer structure at the bottom surface for rays incident from the substrate. The transfer-matrix method can be separately applied to calculate the reflectance and transmittance at the top and bottom surfaces of the wafer, by neglecting the absorption of silicon. The absorption of silicon can be taken into consideration by introducing the internal transmittance $\tau_i = \exp\left(-\dfrac{4\pi\kappa_s d_s}{\lambda\cos\theta_s}\right)$. Here, κ_s is the extinction coefficient of silicon, d_s is the thickness, and θ_s is the angle of refraction. The angle of refraction is complex due to absorption. For a slightly absorbing medium with $\kappa_s << 1$, however, θ_s can be determined using Snell's law by neglecting absorption [11]. Consequently, the radiative properties of the silicon wafer with thin-film coatings in the semitransparent region can be expressed as [12]:

$$\rho = \rho_{ta} + \frac{\tau_i^2 \tau_t^2 \rho_{bs}}{1 - \tau_i^2 \rho_{ts} \rho_{bs}} \tag{3a}$$

$$\tau = \frac{\tau_i \tau_t \tau_b}{1 - \tau_i^2 \rho_{ts} \rho_{bs}} \tag{3b}$$

and

$$\varepsilon = 1 - \rho - \tau \tag{3c}$$

3. Optical Constants of Silicon and Related Materials

The optical constants, including the refractive index (n) and the extinction coefficient (κ), of a material are complicated functions of the wavelength and temperature. They also depend on the crystalline structure as well as doping and impurity levels. In the present version of **Rad-Pro**, carefully selected empirical expressions are used to calculate the optical constants of lightly doped silicon (doping concentration $\leq 10^{15}\ \mathrm{cm}^{-3}$). On the other hand, the Drude model is employed to consider the doping effects on the optical constants of silicon. Consequently, **Rad-Pro** allows the user to select the optical model of silicon between the empirical models for lightly doped silicon and the Drude model for doped silicon with any dopant concentration.

Measurement data of the optical constants of silicon over wide wavelength regions at room temperature can be found in the handbook edited by Palik [13]. However, fewer experimental data exist at high temperatures. Sato [14] was the first to comprehensively study the emittance of silicon wafers by a direct measurement as well as by deducing it from the reflectance and transmittance measurements in the temperature range between room temperature and 800 °C. However, the refractive index values based on his experimental data are consistently higher than those obtained from recent studies. In this section, several expressions of the optical constants of lightly doped silicon are reviewed, and the Drude model will be discussed in detail.

Empirical Models for the Optical Constants of Lightly Doped Silicon

(1) The Refractive Index of Silicon

Jellison and Modine [15] measured the ratio of the Fresnel reflection coefficients of silicon wafers in both polarization states with a two-channel spectroscopic ellipsometer in the temperature range from 25 °C to 490 °C. From the measurement results, they extracted the

refractive index and extinction coefficient using the least-squares Levenberg-Marquardt fitting. The Jellison and Modine (J-M) expression of the refractive index for wavelengths between 0.4 μm and 0.84 μm is given as

$$n_{JM}(\lambda, T) = n_0(\lambda) + \beta(\lambda) T \tag{4}$$

where $$n_0 = \sqrt{4.565 + \frac{97.3}{3.648^2 - (1.24/\lambda)^2}}$$

and $$\beta(\lambda) = -1.864 \times 10^{-4} + \frac{5.394 \times 10^{-3}}{3.648^2 - (1.24/\lambda)^2}$$

where λ [μm] is the wavelength in vacuum and T [°C] is the temperature. These units will be used throughout this document for all expressions.

Li [16] extensively reviewed the refractive index of silicon. By carefully analyzing published experimental data, he developed a functional relation, based on the modified Sellmeier type dispersion relation, for the refractive index of silicon that covers the wavelength region between 1.2 μm and 14 μm and the temperature range up to 480 °C. In Li's original expression, the temperature unit was K, and in the following equations, we have converted it to °C.

$$n_L(\lambda, T) = \sqrt{\varepsilon_r(T) + \frac{g(T)\eta(T)}{\lambda^2}} \tag{5}$$

where $$\varepsilon_r(T) = 11.631 + 1.0268 \times 10^{-3} T + 1.0384 \times 10^{-6} T^2 - 8.1347 \times 10^{-10} T^3$$

$$g(T) = 1.0204 + 4.8011 \times 10^{-4} T + 7.3835 \times 10^{-8} T^2$$

and $$\eta(T) = \exp(1.786 \times 10^{-4} - 8.526 \times 10^{-6} T - 4.685 \times 10^{-9} T^2 + 1.363 \times 10^{-12} T^3)$$

Magunov [17] and Magunov and Mudrov [18] measured the temperature dependence of the refractive index at 1.15 μm and 3.39 μm, and empirically approximated measurement results and built a relation that covers the wavelength region between 0.6 μm and 10 μm, in the

temperature range from room temperature to 430 °C. The Magunov and Mudrov (M-M) expression is

$$n(\lambda,T) = 3.413 + 1.782\times10^{-4}T + 4.365\times10^{-8}T^2 + (0.1635 + 2.400\times10^{-5}T + 1.389\times10^{-7}T^2)\ \lambda^{-2.33} \quad (6)$$

To calculate the refractive index of silicon, **Rad-Pro** uses the J-M expression in the wavelength region from 0.5 μm to 0.84 μm, and Li's expression at wavelengths above 1.2 μm. In the wavelength range between 0.84 μm and 1.2 μm, we use a weighted average based on the extrapolation of the two expressions

$$n_{AVG} = \frac{(1.2-\lambda)n_{JM} + (\lambda-0.84)n_L}{1.2-0.84} \quad (7)$$

where n_{JM} is the refractive index extrapolated from the J-M expression, n_L is from the Li expression, and again λ is in μm. By taking the weighted average of the extrapolated expressions as given in Eq. (7), the predicted radiative properties of silicon will be

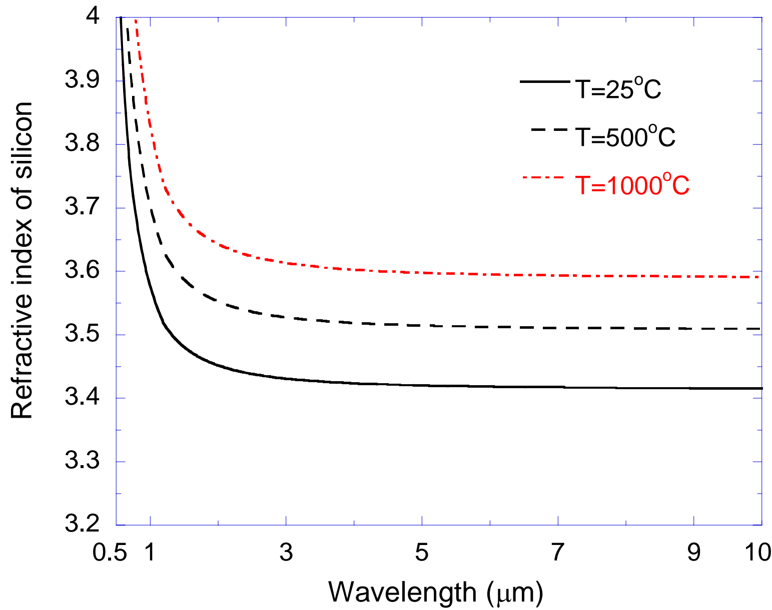

Fig. 3 Calculated refractive index of silicon at selected temperatures

continuous between 0.5 μm and 10 μm. Therefore, the discontinuity in the predicted radiative properties that is observed in the *Multi-RAD* can be removed [5]. Notice that beyond 6 μm or so, lattice vibration causes additional absorption; however, its effects can be neglected due to the weakness of the phonon oscillators in silicon. Figure 3 shows the calculated refractive index of silicon in the wavelength range from 0.5 μm to 10.0 μm at selected temperatures. In general, the refractive index of silicon decreases as the wavelength increases and the temperature decreases. When $\lambda > 10.0$ μm, the refractive index of Si is assumed to be independent of the wavelength, and the value of $n_L(\lambda = 10, T)$ is used to represent the refractive index of Si at any temperature T for $\lambda > 10.0$ μm.

(2) The Extinction Coefficient of Silicon

The extinction coefficient (κ) and absorption coefficient (α) are related by $\alpha = 4\pi\kappa/\lambda$. The absorption coefficient of silicon depends on the absorption processes, such as interband transition, intraband transition, and free-carrier absorption. When the photon energy is higher than the band gap energy of silicon, electrons in the valance band can be excited to the conduction band, resulting in a large absorption coefficient. The J-M expression of the extinction coefficient, covering the wavelength range from 0.4 μm to 0.84 μm, is given as [15]:

$$\kappa_{JM}(\lambda, T) = k_0(\lambda) \exp\left[\frac{T}{369.9 - \exp\left(-12.92 + 6.831/\lambda\right)}\right] \tag{8}$$

where $$k_0(\lambda) = -0.0805 + \exp\left[-3.1893 + \frac{7.946}{3.648^2 - (1.24/\lambda)^2}\right]$$

The absorption coefficient can be deduced from the extinction coefficient.

In the longer wavelength region, Timans [19] measured the emission spectra of several silicon wafers and deduced the absorption coefficient in the wavelength region from 1.1 μm to 1.6 μm, in the temperature range between 330 °C and 800 °C. He suggested that the absorption coefficient can be expressed as a summation of the band gap absorption and free-carrier absorption as following

$$\alpha(\lambda,T) = \alpha_{BG}(\lambda,T) + \alpha_{FC}(\lambda,T) \tag{9}$$

The expression for the band gap absorption can be found in the work by MacFalane et al. [20] and is given by

$$\alpha_{BG}(\lambda,T) = \sum_{i=1}^{4} \alpha_{a,i}(\lambda,T) + \sum_{i=1}^{2} \alpha_{e,i}(\lambda,T) \tag{10}$$

Notice that silicon is an indirect-gap semiconductor and the absorption process is accompanied by either the absorption of a phonon, denoted by $\alpha_{a,i}(\lambda,T)$, or the emission of a phonon, denoted by $\alpha_{e,i}(\lambda,T)$. Detailed expressions for $\alpha_{a,i}(\lambda,T)$ and $\alpha_{e,i}(\lambda,T)$ can be found in Timans [12,19]. The band-gap absorption disappears at wavelengths longer than that corresponding to the energy gap (modified by the phonon energy).

For the free-carrier absorption, Sturm and Reaves [21] suggested an expression based on their measurement of the transmission of the wafer at 1.30 μm and 1.55 μm and in the temperature range of 500 °C to 800 °C. The Sturm and Reaves (S-R) expression is

$$\alpha_{FC} = N_e A_e + N_h A_h \tag{11}$$

where N_e and N_h are electron and hole concentrations, and A_e and A_h are electron and hole absorption cross sections, respectively. The S-R expression agrees well with experimental results in the wavelength region between 1.0 μm and 1.5 μm, but departs from experiments at longer wavelengths. Vandenabeele and Maex [22] studied the free-carrier absorption of silicon in the

infrared region by measuring the emission from the double-side-polished silicon wafers at the wavelengths of 1.7 μm and 3.4 μm, in the temperature range from 400 °C to 700 °C. They proposed a semi-empirical relation for calculating the extinction coefficient as functions of wavelength and temperature due to free-carrier absorption. The Vandenabeele and Maex (V-M) expression is

$$\alpha_{FC}(\lambda,T) = 4.15\times10^{-5}\lambda^{1.51}(T+273.15)^{2.95}\exp\left(\frac{-7000}{T+273.15}\right) \tag{12}$$

Here again, T is in °C. Rogne et al. [23] demonstrated that the absorption coefficient calculated from the V-M expression agrees well with experimental data in the wavelength region between 1.0 μm and 9.0 μm at elevated temperatures.

In the wavelength region between 6.0 μm and 25.0 μm, lattice vibrations causes an additional absorption. Since the effect of lattice absorption is negligible in most RTP applications compared to the absorption by free carriers, it is assumed to be independent of the temperature and dopant concentration. The extinction coefficient for lightly doped silicon due to the lattice absorption is simply obtained from the tabulated extinction coefficient values given in Ref. [13] at room temperature.

In **Rad-Pro**, the absorption coefficient of lightly doped silicon is determined from the J-M expression at $\lambda < 0.9$ μm and from the Timans expression combined with V-M expression for the free-carrier absorption at $\lambda \geq 0.9$ μm. Figure 4 shows the calculated extinction coefficient of silicon in the wavelength range from 0.5 μm to 9.0 μm at selected temperatures. Notice that unlike the refractive index of silicon, there exists a discontinuity in the calculated extinction coefficient especially at the elevated temperatures because the functional expression is changed at λ=0.9 μm. The existence of the absorption edge is clearly seen from the figure, and the

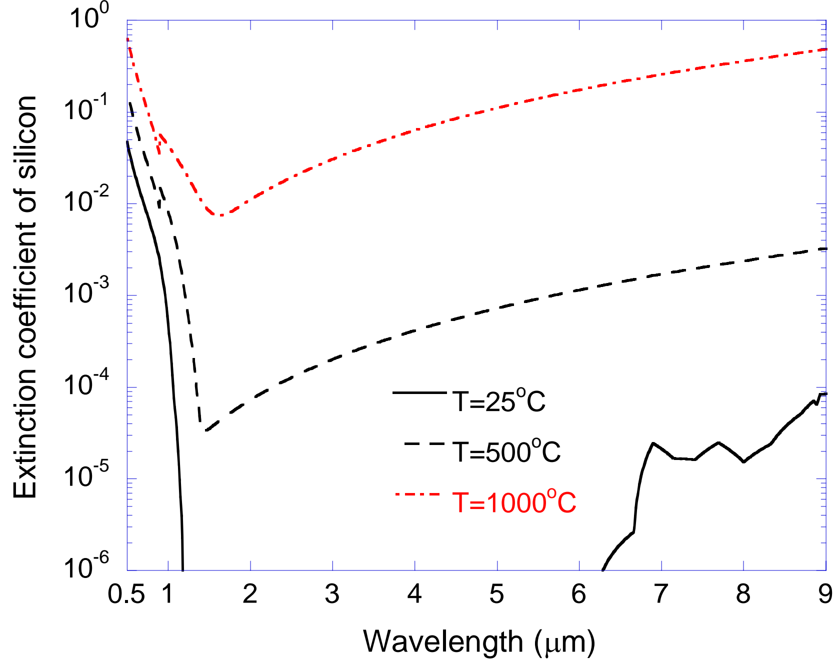

Fig. 4 Calculated extinction coefficient of silicon at selected temperatures

extinction coefficient generally increases as the temperature increases. Since the V-M expression is applicable up to 9.0 μm, the empirical models for the extinction coefficient of lightly doped silicon are inevitably limited to the wavelengths less than 9.0 μm.

The Drude Model for the Optical Constants of Doped Silicon

The complex dielectric function is related to the refractive index (n) and the extinction coefficient (κ) by $\varepsilon(\omega) = (n + i\kappa)^2$. To account for the doping effects, the Drude model is employed, and the dielectric function of both intrinsic and doped silicon is expressed as the following form [5,12]:

$$\varepsilon(\omega) = \varepsilon_{bl} - \frac{N_e e^2 / \varepsilon_0 m_e^*}{\omega^2 + i\omega / \tau_e} - \frac{N_h e^2 / \varepsilon_0 m_h^*}{\omega^2 + i\omega / \tau_h} \tag{13}$$

where the first term in the right (i.e., ε_{bl}) accounts for contributions by transitions across the band gap and lattice vibrations, the second term is the Drude term for transitions in the conduction band (free electrons), and the last term is the Drude term for transitions in the valence band (free holes). Here, N_e and N_h are the concentrations, m_e^* and m_h^* the effective masses, and τ_e and τ_h the scattering times for free electrons and holes, respectively, and e is the electron charge. For simplicity, the effective masses are assumed to be independent of the frequency, dopant concentration, and temperature in the present study, and their values are taken from Ref. [24] as $m_e^* = 0.27m_0$ and $m_h^* = 0.37m_0$, where m_0 is the electron mass in vacuum.

Since ε_{bl} accounts for all contributions other than the free carriers, it can be determined from the refractive index and extinction coefficient of silicon as $\varepsilon_{bl} = (n_{bl} + i\kappa_{bl})^2$, assuming that no free carriers exist [12]. When considering the contribution from transitions across the band gap, the modification of the band structure by impurities is neglected and this assumption should not cause significant error [5]. In the present version, the expression of Jellison and Modine [15] is used to calculate the refractive index n_{bl} in the wavelength region from 0.5 μm to 0.84 μm, and Li's expression [16] is used for wavelengths above 1.2 μm. In the wavelength range between 0.84 μm and 1.2 μm, a weighted average based on the extrapolation of above two expressions is used as suggested by Lee et al. [7]. When $\lambda > 10$ μm, it is assumed that n_{bl} is independent of the wavelength, and the value calculated from Li's expression at $\lambda = 10$ μm and corresponding temperature is used to represent n_{bl} for $\lambda > 10$ μm. It should be noted that the refractive index is not affected by the phonon absorption band between 6 μm and 25 μm.

The extinction coefficient κ_{bl} accounts for the band gap absorption as well as the lattice absorption. The band gap absorption occurs when the photon energy is greater than the band gap energy of silicon and results in a large absorption coefficient. The absorption coefficient is related to the extinction coefficient as $\alpha = 4\pi\kappa/\lambda$, and κ_{bl} can be determined for all temperatures from the equation for absorption coefficients. As a result, when $\lambda < \lambda_g$ where λ_g is the wavelength of the photon, whose energy corresponds to the band gap energy, the extinction coefficient of silicon is calculated from Jellison and Modine's expression in the wavelength range from 0.4 to 0.9 μm, and κ_{bl} is obtained by Timans' expression [19] that is based on the work of MacFarlane et al. [20] in wavelengths greater than 0.9 μm. On the other hand, the lattice absorption occurs in the wavelength range between 6 μm and 25 μm. As done before in empirical models for lightly doped silicon, κ_{bl} due to lattice absorption is obtained from the tabulated data [13].

Once ε_{bl} is determined from the preexisting functional expressions and tabulated data, the remaining parameters are the carrier concentrations and scattering times, which are functions of the temperature and dopant concentration. The calculation of carrier concentrations requires the knowledge of the Fermi energy (E_F). By knowing the Fermi energy, carrier concentrations can be obtained from the following equations [25]

$$N_e = N_C F_{1/2}\left(\frac{E_F - E_g}{kT}\right) \tag{14a}$$

and

$$N_h = N_V F_{1/2}\left(\frac{-E_F}{kT}\right) \tag{14b}$$

where N_C and N_V are the effective density of states in the conduction and valence band, respectively, $F_{1/2}$ is a Fermi-Dirac integral of order ½, E_g is the band gap energy and given by $E_g = 1.17 - 0.000473T^2/(T + 636)$ eV [26], and k is Boltzmann's constant. The values for the effective density of states at room temperature are found in more recent book of Sze [27] as $N_C = 2.86 \times 10^{19}$ cm^{-3} and $N_V = 2.66 \times 10^{19}$ cm^{-3}, respectively, and the temperature dependence of $T^{1.5}$ is considered for both N_C and N_V. The Fermi-Dirac integral $F_{1/2}$ can be simplified by an exponential, and the procedures described in Ref. [25] are used to determine Fermi energy satisfying charge neutrality, which is expressed as

$$N_h + N_D^+ = N_e + N_A^- \tag{15}$$

where N_D^+ and N_A^- are ionized donor and acceptor concentration, respectively. In the calculation of carrier concentrations, the ionization energy of the considered impurity or dopant is required. Phosphorus and boron are default impurities for *n*-type and *p*-type, respectively in the current version of the software. The ionization energies of phosphorus and boron are assumed to be independent of dopant concentration and temperature, and their vales are taken as 44 meV and 45 meV, respectively from the Ref. [28]. The calculated results of carrier concentrations N_e and N_h at a given dopant concentration and temperature are within 3% of the values obtained by numerical integration.

The scattering time τ_e or τ_h depends on the collisions of electrons or holes with lattice (phonons) and ionized dopant sites (impurities or defects); hence, it generally depends on the temperature and dopant concentration. The total scattering time (for the case of τ_e), which consists of the above two mechanisms, can be expressed as [28]

$$\frac{1}{\tau_e} = \frac{1}{\tau_{e-l}} + \frac{1}{\tau_{e-d}} \tag{16}$$

where τ_{e-l} and τ_{e-d} denote the electron-lattice and electron-defect scattering time, respectively. Similarly, τ_h can be related to τ_{h-l} and τ_{h-d}. In addition, the scattering time τ is also related to the mobility μ by $\tau = m^* \mu / e$. At room temperature, the total scattering time τ_e^0 or τ_h^0, which depends on the dopant concentration, can be determined from the fitted mobility equations [29]

$$\mu_e^0 = \frac{1268}{1 + (N_D / 1.3 \times 10^{17})^{0.91}} + 92 \tag{17a}$$

and

$$\mu_h^0 = \frac{447.3}{1 + (N_A / 1.9 \times 10^{17})^{0.76}} + 47.7 \tag{17b}$$

where superscript 0 indicates values at 300 K and N_D or N_A is the dopant concentration of donor (phosphorus, *n*-type) or acceptor (boron, *p*-type) in cm^{-3}. On the other hand, the scattering time from lattice contribution τ_{e-l}^0 or τ_{h-l}^0, which is independent of the dopant concentration, can be separately obtained from the room temperature lattice mobility of 1451 $\text{cm}^2 \cdot \text{V}^{-1} \cdot \text{s}^{-1}$ for electrons or 502 $\text{cm}^2 \cdot \text{V}^{-1} \cdot \text{s}^{-1}$ for holes [30]. Consequently, the scattering time from impurity contribution τ_{e-d}^0 or τ_{h-d}^0 can be determined from Eq. (15) by knowing the total scattering time and that due to lattice contribution. At room temperature, the scattering process is dominated by lattice scattering for lightly doped silicon, and the impurity scattering becomes important for heavily doped silicon when the dopant concentration exceeds 10^{18} cm^{-3}.

For the temperature dependence of the scattering time, theory predicted that the carrier-impurity scattering times vary with $T^{1.5}$, and the carrier-lattice scattering times due to acoustic phonons vary with $T^{-1.5}$ [28]. As the temperature increases, the scattering rate ($1/\tau$) due to

impurity tends to decrease because the electrostatic force that governs dopant sites becomes weaker and carriers can move more agilely. On the other hand, the carrier-lattice scattering rate increases as the temperature goes up because of the increased phonon density of states. Therefore, lattice scattering dominates the scattering process at high temperatures even for heavily doped silicon. Because of the relatively insignificance of impurity scattering at high temperatures, the following formula will be used to calculate the impurity scattering times:

$$\frac{\tau_{e-d}}{\tau_{e-d}^{0}} = \frac{\tau_{h-d}}{\tau_{h-d}^{0}} = \left(\frac{T}{300}\right)^{1.5} \tag{18}$$

where T is in K. The temperature dependence of τ_{e-l} and τ_{h-l} can be more complicated since optical phonon modes may contribute to the scattering in addition to acoustic phonon modes. Morin and Maita [30] fitted the mobility with experiments and indicated that the mobility due to lattice scattering varies as $T^{-2.6}$ for electrons and $T^{-2.3}$ for phonons. In order to obtain a better agreement with the measured near-infrared absorption coefficients for lightly doped silicon [5,12,21-23], the expressions for lattice scattering are modified in the present study, as follows:

$$\tau_{e-l} = \tau_{e-l}^{0} \left(T/300\right)^{-3.8} \tag{19a}$$

and

$$\tau_{h-l} = \tau_{h-l}^{0} \left(T/300\right)^{-3.6} \tag{19b}$$

Substituting Eqs. (18) and (19) into Eq. (16) gives the scattering time for any temperature and dopant concentration.

Optical Constants of Other Materials

Due to lack of experimental data, assumptions have to be made for the optical constants of other materials, such as silicon dioxide, silicon nitride, and polysilicon as commonly done in the literature [5,12]. The optical constants of silicon dioxide and silicon nitride are mainly based

on the data collected in Palik's handbook [31,32] and assumed to be independent of temperature. In the wavelength range between 0.3 μm and 25.0 μm, the optical constants of silicon dioxide are tabulated from Palik's handbook, and linear interpolation is used to get values in between two data points. For silicon nitride, the same procedure is used to obtain the optical constants in the wavelength range between 0.2 μm and 1.24 μm. When $\lambda > 1.24$ μm, a constant value of 1.998 is used for the refractive index of silicon nitride, and the extinction coefficient is assumed to be zero.

The optical constants of polysilicon may be different from those of single-crystal silicon because of the presence of the grain boundaries. The main difference between polysilicon and single-crystal silicon is that the absorption edge of polysilicon is broader due to the additional long-wavelength absorption [33]. The refractive index is slightly higher and the extinction coefficient is several times greater than those of single-crystal silicon at wavelengths shorter than the band gap wavelength, but the differences become smaller at longer wavelengths [12,34,35]. However, the characteristic of polysilicon depends largely on the grain structure resulting from different deposition conditions. In the present version of **Rad-Pro**, the optical constants of polysilicon are assumed to be the same as those of single-crystal silicon.

Comparison with Room Temperature reflectance Measurements

An experimental validation was performed on the model expressions for the refractive index of silicon and related materials at room temperature. The reflectance was measured over the wavelength region from 0.5 μm to 1.0 μm for five samples and compared with the calculated values using thin-film optics. The excellent agreement between the measured and calculated reflectance suggests that the extrapolation of the expressions for the refractive index of silicon to

the wavelength region between 0.84 μm and 1.0 μm is appropriate at room temperature. In addition, the excellent agreement in the reflectance minimum, which is independent of the coating thickness when only one film is coated, confirms the expressions for the optical constants of silicon dioxide and silicon nitride. The calculated reflectance spectrum was fitted to the measured values by changing the thickness of the thin-film coatings. This allows accurate determination of the coating thickness for single-layer coatings. However, a larger deviation exists for a silicon wafer coated with polysilicon and silicon oxide films, suggesting that further study about the optical constants of polysilicon is needed. The detailed information about the comparison with the reflectance measurements can be found in Ref. [7].

4. Getting Started

Installation of Files

Rad-Pro was developed using VBA programming in Excel. All of the calculation modules are provided in the form of a dynamic link library (DLL), and the main program in the Excel spreadsheet can accept input parameters from users as well as show the calculated results. In order to run **Rad-Pro**, the DLL file (module.dll) should be located in a default folder (i.e., C:\Rad-Pro\). Copy the provided library file into the folder. Notice that the folder name should be the same as specified above to properly run the software. On the other hand, the Excel file (Rad-Pro.xls) can be located in any folder. Users can start the program by double clicking Rad-

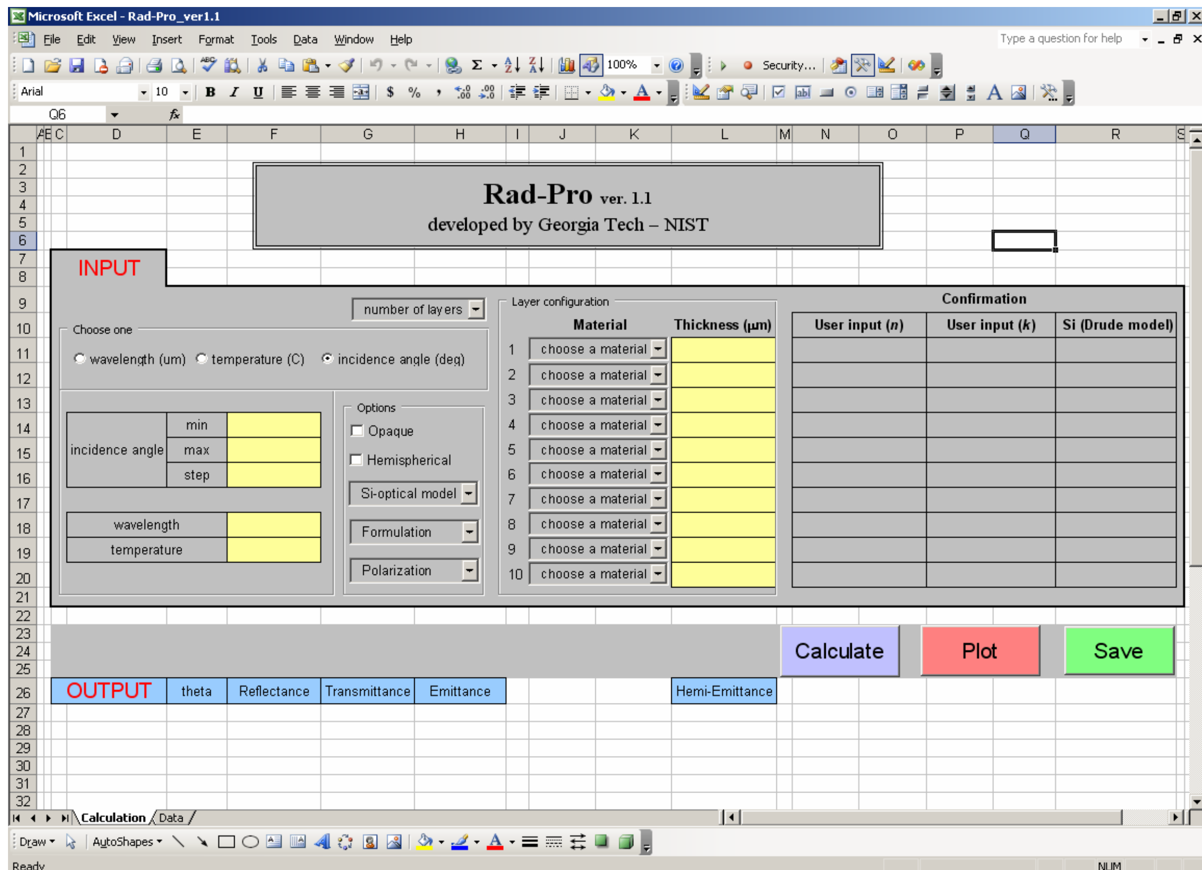

Fig. 5 Rad-Pro layout when it is started

Pro.xls. Figure 5 shows the layout when it is initialized. If the security level for the macro in Excel is set to *high*, make sure that it should be changed to *low* or *medium* before running **Rad-Pro** by clicking on Options in the Tools menu of Excel. At the bottom of the Options window, click on Macro Security. In the Security Level Tab, select either Medium or Low option button, and click OK twice.

Input Parameters

Rad-Pro requires several input parameters, and inputting methods include: option button, check box, combo box, and cells with the light-yellow color (Fig. 6). The option button allows the user to choose the type of input parameters: wavelength, temperature, or incidence angle. Detailed descriptions about the input parameters will be provided later. Using the check box, the user can activate an opaque or hemispherical option. The combo box allows the user to select one item from the list: number of layers, optical model for Si, polarization status, calculation methods, and material for each layer. Furthermore, **Rad-Pro** also takes values directly from the Excel worksheet. The user should input correct values in the light-yellow cells only.

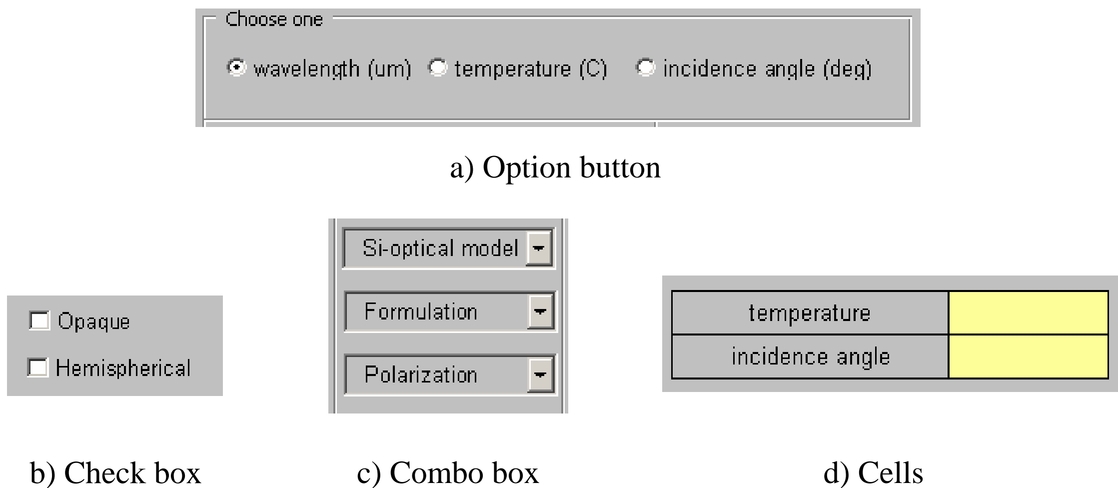

a) Option button

b) Check box c) Combo box d) Cells

Fig. 6 Examples of the option button, check box, combo box, and cells

These values will be used for the calculation. The gray colored cells, however, are for information purposes only and do not affect the calculated results.

Wavelength, temperature, and incidence angle

To facilitate graphing, the radiative properties of multilayer structure can be evaluated as a function of a single variable, selected from the option button: wavelength, temperature, or incidence angle. Figure 7 shows three possible cases. As shown in Fig. 7a, if wavelength is selected, the text in the largest gray-colored cell under the option button will immediately change to the word "wavelength" indicating that the wavelength dependence of the radiative properties will be calculated. The user can define the wavelength range by entering the values of

a) Wavelength dependence

b) Temperature dependence

c) Incidence angle dependence

d) Input values in the cells

Fig. 7 Option buttons for wavelength, temperature, and incidence angle dependence

the wavelength minimum, maximum, and step size in the light-yellow cells. Beneath these cells, two more cells accept the values for the temperature and angle of incidence if the wavelength is selected. For example, if the user wants to calculate the radiative properties in the wavelength range from 0.5 μm to 1.0 μm in increment of 0.001 μm at a temperature of 25 °C and incidence angle of 30°, the user should choose the wavelength option button and enter values for the wavelength range, temperature, and angle of incidence as illustrated in Fig. 7d. Notice that the units for the wavelength, temperature, and incidence angle are micrometer, degree Celsius, and degree, respectively.

Optical model of Si

Rad-Pro allows the user to select the optical model of Si between the empirical model and the Drude model as explained in section 3. Selection of the optical model of Si (Fig. 8) must be performed before layer configuration. Once the user selects the model, it will be consistently applied to all Si layer of the specified multilayer structure unless the user changes the optical model of Si. If the Drude model is selected, a dialog box that takes input values about the dopant type and concentration will appear whenever Si is chosen during the layer configuration. Inputting the dopant type and concentration will be further discussed in the layer configuration. Notice that the doping effect is not considered for polysilicon. Therefore, the optical constant of polysilicon is always calculated from the empirical expressions for lightly doped silicon.

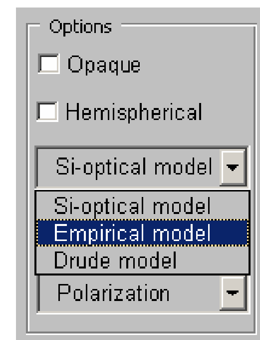

Fig. 8 Selection of the optical model of Si

Layer configuration

The multilayer structure can have up to 10 layers. As explained in Section 2, it is assumed that the electromagnetic wave is incident from air to the first layer (layer 1). For the layer configuration, the number of layers of the structure as well as a material and thickness of each layer should be specified. Notice that before selecting the material of each layer, the user must first specify the number of layers (Fig. 9).

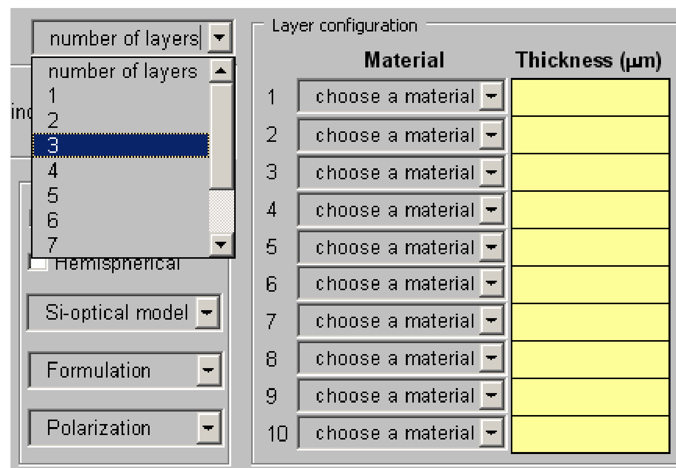

Fig. 9 Selection of the number of layers

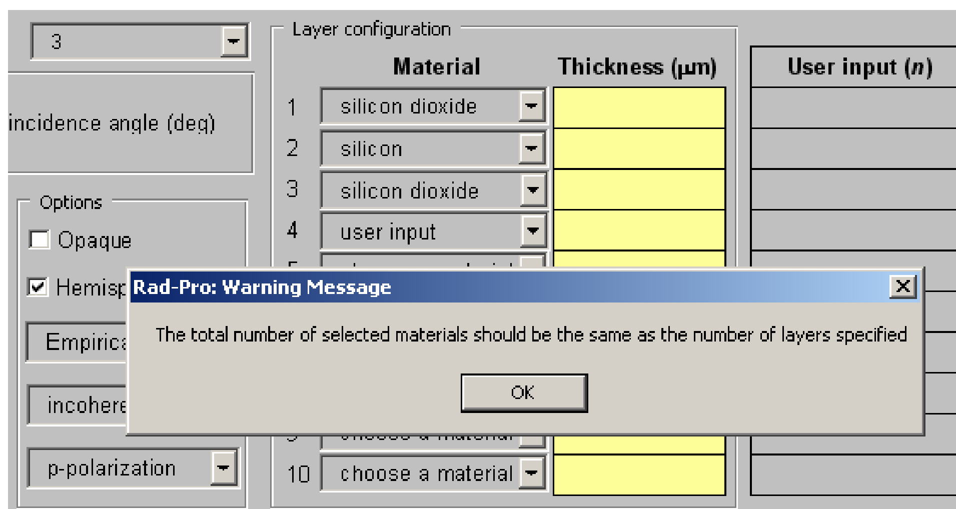

Fig. 10 Selection of the material and an example of the warning message

After selecting the number of layers, the user can choose a material for each layer. **Rad-Pro** provides four materials: silicon, silicon dioxide, silicon nitride, and polysilicon as defaults. In addition, it also provides a way that the user can specify the equation for the optical constants of the user-defined material. In the present version, only a second-order polynomial of the wavelength can be used. If the user tries to select a material of the layers beyond the specified number of layers, a warning message will be shown as illustrated in Fig. 10.

When the user selects "user input" from the material combo box, the dialog box shown in Fig. 11 will prompt the user to input the properties for the user-defined material. In the dialog

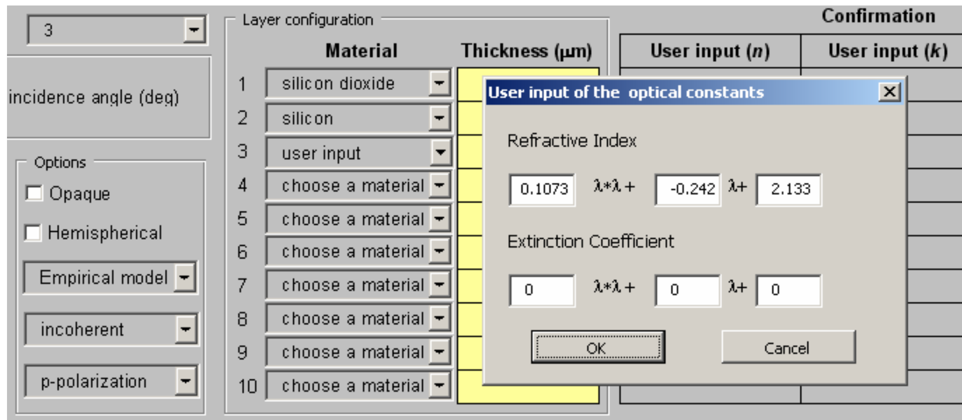

a) Dialog box for user's input of the optical constants

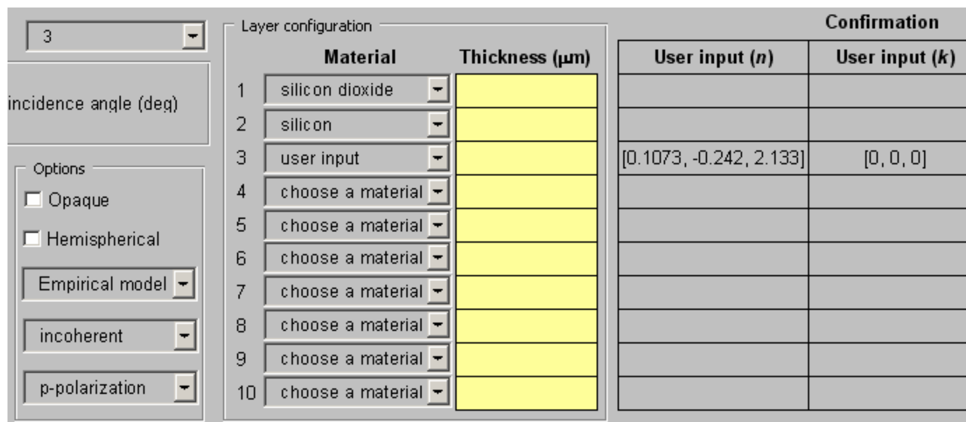

b) Confirmation for the coefficients of polynomial (second-order)

Fig. 11 Using the optional user input for n and κ of the material

box, the user can enter the coefficients of a second-order polynomial for the refractive index and extinction coefficient of the desired material. After entering all coefficients, click the OK button. The coefficients that the user entered in the form will be shown in the gray-colored cells for confirmation. For example, $[a,b,c]$ means that the equation of n or κ will be $a\lambda^2 + b\lambda + c$. If the user wants to change the values of the coefficients, select other materials from the list of the corresponding layer. Then, select "user input" again. A new dialog box for entering the coefficients will appear. Note that the second-order polynomial for the optical constants must be

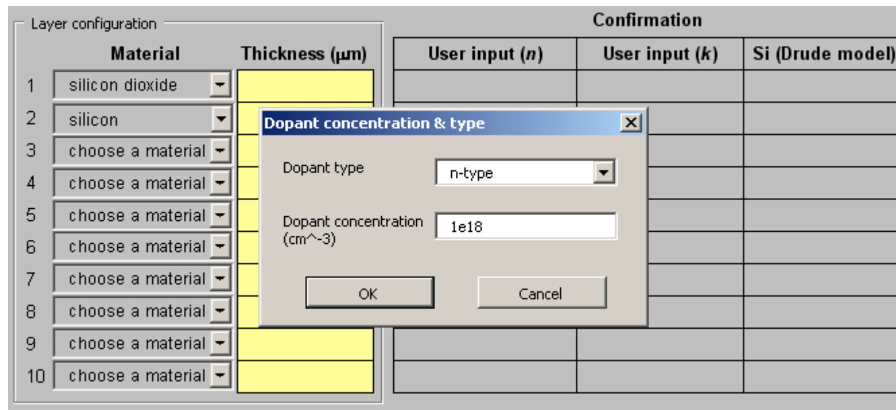

a) Window for the user input of the dopant type and concentration

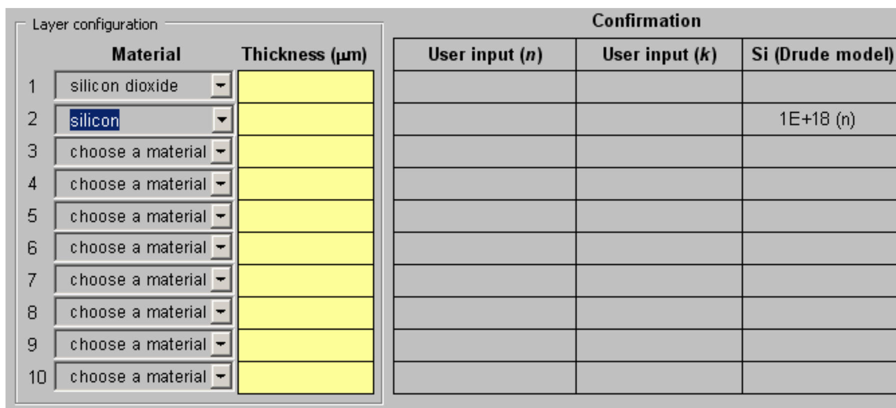

b) Confirmation of the dopant type (e.g., n-type) and concentration (e.g., $1\times10^{18}\ \text{cm}^{-3}$)

Fig. 12 Using the Drude model for doped silicon

well-defined in the wavelength range where the user wants to calculate the radiative properties.

After finishing the selection of the material, the user can enter the thickness of each layer in μm. If the user does not enter the values of the thickness for a certain layer, **Rad-Pro** will regard its thickness as zero. As a result, the final multilayer structure is just like the original structure without the layer having zero thickness.

If "Drude model" is selected in the optical model selection step, the dopant type and concentration of each Si layer must be specified during the layer configuration. Figure 12 shows an example of inputting parameters for the dopant type and concentration. The dopant type can be selected by using the combo box of the dialog box shown in Fig. 12. Notice that if the user chooses intrinsic as the dopant type, only thermally generated free carriers exist in the conduction (electron) or valence (hole) band, and any number typed in the dopant concentration of the dialog box does not affect the calculated results. The way to input and change values for dopant type and concentration is basically the same as the case of user-defined materials.

Formulation

As explained earlier, in order to calculate the radiative properties of the multilayer structure, **Rad-Pro** uses two methods: coherent and incoherent formulation. The coherent formulation is the same as thin-film optics, which considers each layer as a thin film. On the other hand, the incoherent formulation considers the substrate only as incoherent and other coatings as coherent [7,9]. Note that the fringes due to the thin-film coatings are still observable even in the incoherent formulation. The user

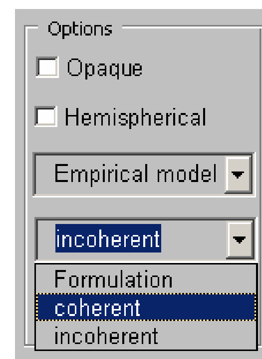

Fig. 13 Selection of the formulation scheme

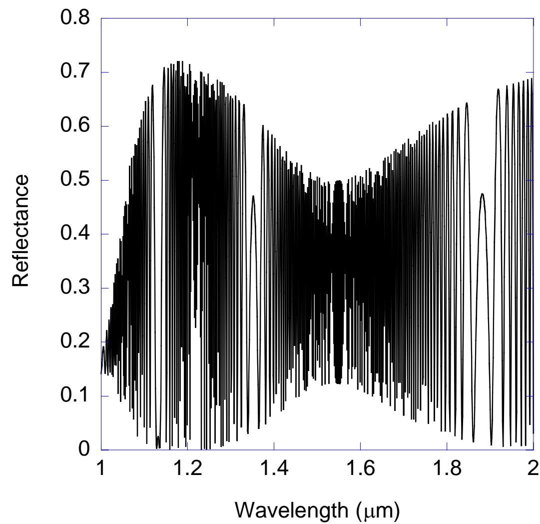

a) Coherent formulation

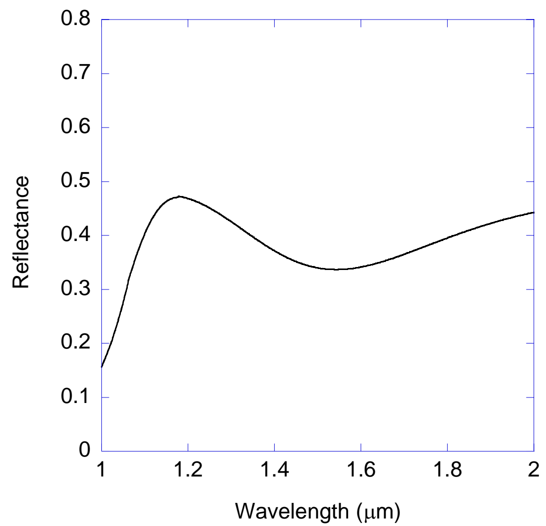

b) Incoherent formulation

Fig. 14 Reflectance of a silicon wafer (500 μm) coated with a silicon dioxide film (0.8 μm) on the top surface

can select either of them from the formulation combo box as shown in Fig. 13. Figure 14 shows the calculated reflectance of a silicon wafer (500 μm) coated with a silicon dioxide film (0.8 μm) on the top surface at room temperature with normal incidence, using coherent or incoherent formulation.

Polarization

Rad-Pro allows the user to change the polarization of the incident radiation. By selecting it from the combo box, the user can easily specify the polarization status. When the incident radiation is unpolarized, the radiative properties are averaged over *p* and *s* polarizations.

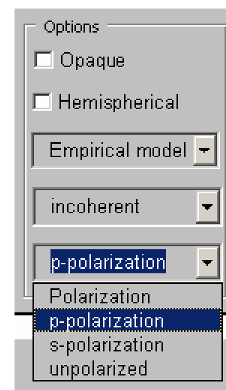

Fig. 15 Selection of polarization of the incident radiation

Opaque substrate

Since most silicon wafers are thick enough to be opaque, especially in the wavelength range between 0.5 μm and 1.0 μm, the silicon substrate can be regarded as a semi-infinite medium. Therefore, the wafer with various thin-film coatings in the opaque region can be modeled as a multilayer structure of thin films. **Rad-Pro** provides an option for this case. In the default setting, the semi-infinite medium at the bottom of the multilayer structure is air. However, if the user clicks the opaque check box, the silicon substrate is treated as the bottom semi-infinite medium instead of air. Therefore, the thin films coated on the bottom surface of the silicon substrate will not be considered for the calculation. Since the interference effects inside the substrate will not be observable with the opaque option, it is not recommended that the incoherent formulation is simultaneously used with the opaque option. Notice that

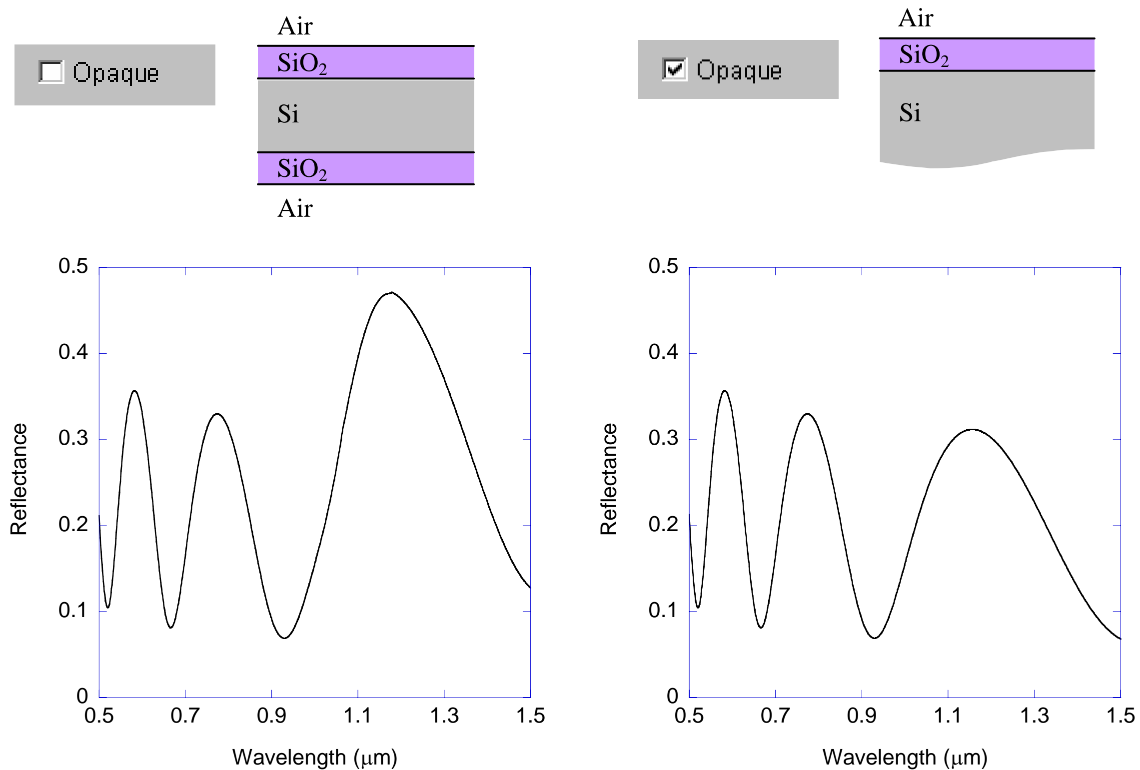

Fig. 16 Reflectance of a silicon wafer (500 μm) coated with silicon dioxide film (0.8 μm) on both sides at room temperature and normal incidence

the transmittance is always zero with the opaque option and thus, the emittance is simply $1-\rho$. Figure 16 shows the calculated reflectance with or without the opaque option for illustration. It is clear that the effects of the silicon dioxide coated at the bottom surface of the Si substrate are not considered when opaque is checked. To enhance clarity, incoherent formulation is intentionally used for the left plot.

Hemispherical emittance

The spectral-hemispherical emittance can be evaluated by activating the hemispherical checkbox as shown in Fig. 17. The spectral-hemispherical emittance is obtained by integrating over the hemisphere:

$$\varepsilon_{\lambda} = 2\int_{0}^{\pi/2} \varepsilon_{\lambda,\theta}(\theta)\cos\theta\sin\theta d\theta \quad (20)$$

where $\varepsilon_{\lambda,\theta}$ is the spectral-directional emittance. Due to the axial symmetry of the planar structure, the emission is assumed to be independent of the azimuthal angle. The electric field for *s* polarization is defined to be parallel to the unit direction vector of the azimuthal angle at any point on the surface. It is important to note that the calculated hemispherical emittance from Eq. (20) is the emittance from the top surface of the multilayer structure (i.e., outward surface of the layer 1) because the radiative properties depend on the side on which electromagnetic waves are incident.

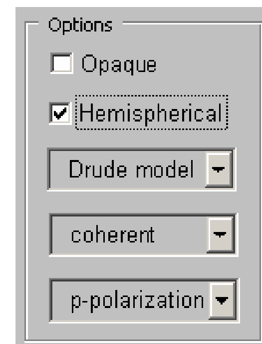

Fig. 17 Calculation of hemispherical emittance

Calculation and Plotting

After entering all of the input parameters, the user can calculate the radiative properties of the specified multilayer structure by clicking the "Calculate" button at right bottom of the screen. The calculated results will be shown in the rows under the blue-colored cells. Consider the following case. The silicon wafer is coated with a 300-nm silicon dioxide layer on both sides. The thickness of silicon wafer is 700 μm, and silicon is doped with phosphorus at $10^{16}\ \text{cm}^{-3}$. To consider the doping effects, the Drude model is used. The temperature of silicon wafer with thin-film coatings is 500 °C, and the electromagnetic waves are incident at $\theta = 0^{\circ}$. The considered wavelength range is from 0.5 μm to 10 μm in every 0.01 μm, and the incoherent formulation is used for calculation. In addition, hemispherical emittance of the specified structure is calculated. The correct values of input parameters and calculated results from **Rad-Pro** are shown in Fig. 18.

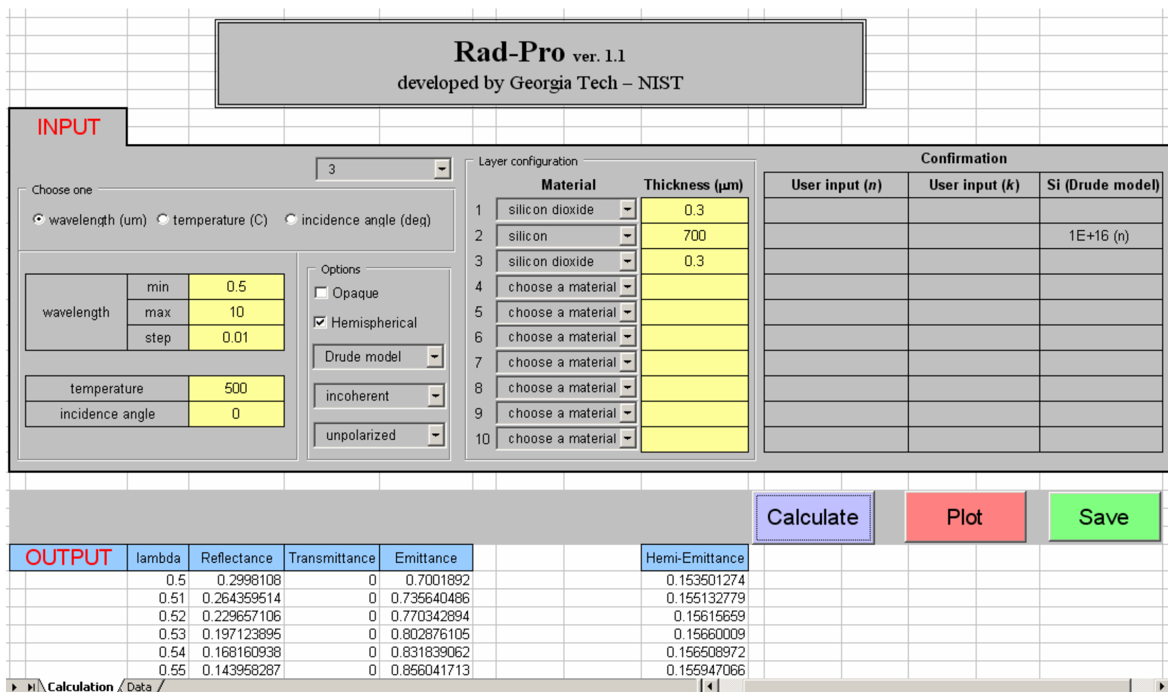

Fig. 18 Calculating the radiative properties of multilayers

Notice that the information about the dopant type (i.e. *n*-type) and concentration of silicon are shown in the gray-colored cell that is located at the same low of the layer 2 (i.e., silicon). The calculation took about 2 min. of CPU time with a Pentium 4 processor (1.8 GHz).

Once the calculation is done, it is possible to generate an *x*-*y* plot of the radiative properties versus wavelength, temperature, or incidence angle. When generating plots in **Rad-Pro**, the "XY (Scatter)" is the default chart type. The user should change the default chart type in Excel to properly use the plot option in **Rad-Pro**. Please refer to the help in Excel for further instructions on how to change the default chart type in Excel. To plot, click the "Plot" button. Figure 19 shows an example for plotting the calculated results with the same parameters as in the case of Fig. 18. To avoid possible confusion, the hemispherical emittance is intentionally not plotted with the spectral-directional radiative properties, and the user can plot it easily if necessary. It should be noted that sometimes the thickness of substrate falls between situations of completely coherent and incoherent, i.e., the partially coherent regime. One can use the coherent

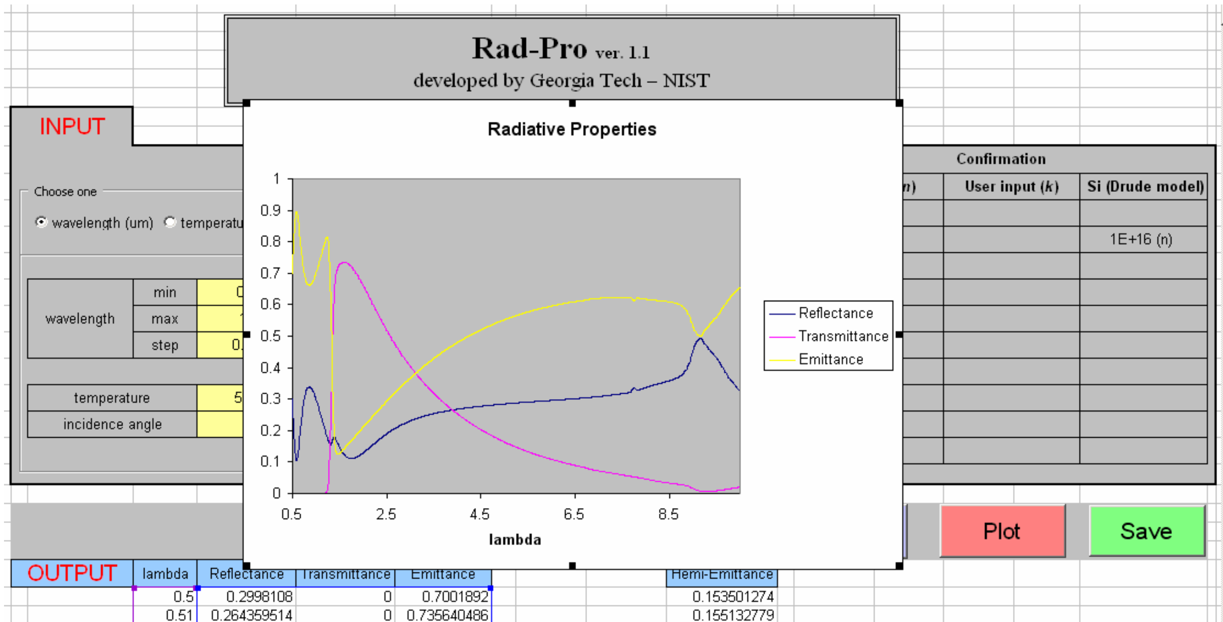

Fig. 19 Plotting the calculated results

formulation to obtain an output file with sufficiently fine data points, and then use the spectral averaging method by following the work of Lee et al. [6] to obtain the radiative properties in the partially coherent situation.

Saving Data

By clicking the “Save” button, the user can save all of the calculated data. There are two spreadsheets inside **Rad-Pro**, named as “Calculation” and “Data”. The spreadsheet named “Calculation” is for calculation only and is activated whenever the program is started. On the other hand, the “Data” spreadsheet is for saving data. Once the user clicks the “Save” button in the “Calculation” spreadsheet, all of the information in the “Calculation” spreadsheet will be transferred into “Data” spreadsheet, and **Rad-Pro** automatically activates the “Data”

Data were saved on	9/19/2005, 9:26:00 AM

INPUT PARAMETERS	
temperature	500
incidence angle	0
Optical Model of Si	Drude model
Formulation Scheme	Incoherent formulation
Polarization	unpolarized
Activated Options	Hemispherical

Material	Thickness	Doping parameter	User input (n)	User Input (k)
Silicon Dioxide	0.3			
Silicon	700	1E+16 (n)		
Silicon Dioxide	0.3			

wavelength	Reflectance	Transmittance	Emittance	Hemi-emittance
0.5	0.2998108	0	0.7001892	0.153501274
0.51	0.264359514	0	0.735640486	0.155132779
0.52	0.229657106	0	0.770342894	0.15615659
0.53	0.197123895	0	0.802876105	0.15660009
0.54	0.168160938	0	0.831839062	0.156508972
0.55	0.143958287	0	0.856041713	0.155947066
0.56	0.125333071	0	0.874666929	0.154988352
0.57	0.112674406	0	0.887325594	0.153703764
0.58	0.105971309	0	0.894028691	0.152171666
0.59	0.104820023	0	0.895179977	0.150470191
0.6	0.10853939	0	0.89146061	0.148665431
0.61	0.116318548	0	0.883681452	0.146809092
0.62	0.127270881	0	0.872729119	0.144948921
0.63	0.140530803	0	0.859469197	0.143123589

Name of spreadsheet

Calculation | Data

Fig. 20 Saving the calculated data

spreadsheet, allowing the user to examine the transferred data. Figure 20 shows an example of saving the data into the “Data” spreadsheet.

Once the user has finished and clicks to exit Excel, the user should understand the implication of choosing Yes, No, or Cancel. If the user chooses “Yes”, the program actually writes over the existing file and saves the current work. Notice that all of the information in the “Calculation” spreadsheet will be lost once the user exits Excel. In other words, **Rad-Pro** will delete all data in the “Calculation” spreadsheet whenever it is started. However, the transferred data into the “Data” spreadsheet will remain. If the user chooses “No”, the program does not save the work, and the data transferred into the “Data” spreadsheet will be lost. Finally, if the user chooses “Cancel”, the user will be back to the program. Alternatively, to save the file as a new name, the user should click Save As under the File menu and choose a new filename.

5. Proposed Future Enhancements

The experiment validation about the predicted results using **Rad-Pro** is a very important but challenging task, especially at elevated temperatures. A facility is being developed to measure the radiative properties at elevated temperatures [4]. With this facility, the functional expression for the optical constants of silicon and relevant materials can be thoroughly examined over the wide temperature ranges. To account for the doping effects, the simple Drude model is incorporated into **Rad-Pro**; however, experimental validation of the model must be performed over a wide range of the doping concentration. As suggested by Lee et al. [7], further work is also needed to investigate the optical constants of polysilicon film deposited under various conditions. In addition, the optical constants of emerging high-κ dielectrics such as HfO_2 [36] and ZrO_2 [37] can be studied and included in future versions of **Rad-Pro**.

Acknowledgments

This work was made possible by the financial support from the NIST Office of Microelectronics Program and the National Science Foundation. The authors would like to thank Drs. Benjamin Tsai and Leonard Hanssen for valuable suggestions on the software, and Drs. Edward Early and Kenneth Kreider for their help in the reflectance measurements. The authors are also grateful to late Professor David DeWitt for initiating this effort.

References

[1] P. J. Timans, R. Sharangpani, and R. P. S. Thakur, "Rapid Thermal Processing," *Handbook of Semiconductor Manufacturing Technology*, Y. Nishi and R. Doering (eds.), Marcel Dekker, Inc., New York (2000), pp. 201-286.

[2] Z. M. Zhang, "Surface Temperature Measurement Using Optical Techniques," *Annual Review of Heat Transfer*, vol. **11**, C. L. Tien (ed.), Begell House, New York (2000), pp. 351-411.

[3] Y. H. Zhou, Y. J. Shen, Z. M. Zhang, B. K. Tsai, and D. P. DeWitt, "A Monte Carlo Model for Predicting the Effective Emissivity of the Silicon Wafer in Rapid Thermal Processing Furnaces," *Int. J. Heat Mass Transfer*, vol. **45** (2002), pp. 1945-1949.

[4] B. K. Tsai, D. P. DeWitt, E. A. Early, L. M. Hanssen, S. N. Mekhontsev, M. Rink, K. G. Kreider, B. J. Lee, and Z. M. Zhang, "Emittance Standards for Improved Radiaion Thermometry During Thermal Processing of Silicon Materials," *9th International Symposium on Temperature and Thermal Measurements in Industry and Science*, Cavtat-Dubrovnik, Croatia, 2004.

[5] J. P. Hebb, "Pattern Effects in Rapid Thermal Processing," Ph.D. Dissertation, Department of Mechanical Engineering, Massachusetts Institute of Technology, Cambridge, MA (1997).

[6] B. J. Lee, V. P. Khuu, and Z. M. Zhang, "Partially Coherent Spectral Transmittance of Dielectric Thin Films with Rough Surfaces," *J. Thermophys. Heat Transfer*, vol. **19** (2005), pp. 360-366.

[7] B. J. Lee, Z. M. Zhang, E. A. Early, D. P. DeWitt, and B. K. Tsai, "Modeling Radiative Properties of Silicon with Coatings and Comparison with Reflectance Measurements," *J. Thermophys. Heat Transfer* (2005), in press.

[8] P. Yeh, *Optical Waves in Layered Media*, Wiley, New York (1988).

[9] Z. M. Zhang, C. J. Fu, and Q. Z. Zhu, "Optical and Thermal Radiative Properties of Semiconductors Related to Micro/Nanotechnology," *Adv. Heat Transfer*, vol. **37** (2003), pp. 179-296.

[10] Z. M. Zhang, "Reexamination of the Transmittance Formulae of a Lamina," *J. Heat Transfer*, vol. **119** (1997), pp. 645-647.

[11] Z. M. Zhang, "Optical Properties of a Slightly Absorbing Film for Oblique Incidence," *Appl. Opt.*, vol. **38** (1999), pp. 205-207.

[12] P. J. Timans, "The Thermal Radiative Properties of Semiconductors," *Advances in Rapid Thermal and Integrated Processing*, F. Roozeboon (ed.), Kluwer Academic Publishers, Dordrecht, The Netherlands (1996), pp. 35-101.

[13] D. F. Edwards, "Silicon (Si)," *Handbook of Optical Constants of Solids*, E. D. Palik (ed.), Academic Press, Orlando (1985), pp. 547-569.

[14] T. Sato, "Spectral Emissivity of Silicon," *Jpn. J. Appl. Phys.*, vol. **6** (1967), pp. 339-347.

[15] G. E. Jellison and F. A. Modine, "Optical Functions of Silicon at Elevated Temperatures," *J. Appl. Phys.*, vol. **76** (1994), pp. 3758-3761.

[16] H. H. Li, "Refractive Index of Silicon and Germanium and Its Wavelength and Temperature Derivatives," *J. Phys. Chem. Ref. Data*, vol. **9** (1980), pp. 561-658.

[17] A. N. Magunov, "Temperature-Dependence of Silicon Single Crystal Refractive-Index in the 300-700-K Range," *Opt. Spectrosc.*, vol. **73** (1992), pp. 352-354.

[18] A. N. Magunov and E. V. Mudrov, "Optical-Properties of Lightly Doped Monocrystalline Silicon in Absorption Edge Range at 300-K-700-K," *Opt. Spectrosc.*, vol. **70** (1991), pp. 145-149.

[19] P. J. Timans, "Emissivity of Silicon at Elevated Temperatures," *J. Appl. Phys.*, vol. **74** (1993), pp. 6353-6364.

[20] G. G. Macfarlane, T. P. Mclean, J. E. Quarrington, and V. Roberts, "Fine Structure in the Absorption-Edge Spectrum of Si," *Phys. Rev.*, vol. **111** (1958), pp. 1245-1254.

[21] J. C. Sturm and C. M. Reaves, "Silicon Temperature-Measurement by Infrared Absorption - Fundamental Processes and Doping Effects," *IEEE Trans. Electron Devices*, vol. **39** (1992), pp. 81-88.

[22] P. Vandenabeele and K. Maex, "Influence of Temperature and Backside Roughness on the Emissivity of Si Wafers During Rapid Thermal-Processing," *J. Appl. Phys.*, vol. **72** (1992), pp. 5867-5875.

[23] H. Rogne, P. J. Timans, and H. Ahmed, "Infrared Absorption in Silicon at Elevated Temperatures," *Appl. Phys. Lett.*, vol. **69** (1996), pp. 2190-2192.

[24] W. G. Spitzer and H. Y. Fan, "Determination of Optical Constants and Carrier Effective Mass of Semiconductors," *Phys. Rev.*, vol. **1** (1957), pp. 882-890.

[25] T. K. Gaylord and J. N. Linxwiler, "A Method for Calculating Fermi Energy and Carrier Concentrations in Semiconductors," *Am. J. Phys.*, vol. **44** (1976), pp. 353-355.

[26] C. D. Thurmond, "Standard Thermodynamic Functions for Formation of Electrons and Holes in Ge, Si, Gaas, and Gap," *J. Electrochem. Soc.*, vol. **122** (1975), pp. 1133-1141.

[27] S. M. Sze, *Semiconductor Devices, Physics and Technology*, 2nd ed, Wiley, New York (2002).

[28] S. M. Sze, *Physics of Semiconductor Devices*, 2nd ed, Wiley, New York (1981).

[29] W. E. Beadle, J. C. C. Tsai, and R. D. Plummer, *Quick Reference Manual for Silicon Integrated Circuit Technology*, Wiley, New York (1985).

[30] F. J. Morin and J. P. Maita, "Electrical Properties of Silicon Containing Arsenic and Boron," *Phys. Rev.*, vol. **96** (1954), pp. 28-35.

[31] H. R. Philipp, "Silicon Dioxide (SiO_2)," *Handbook of Optical Constants of Solids*, E. D. Palik (ed.), Academic Press, Orlando (1985), pp. 749-763.

[32] H. R. Philipp, "Silicon Nitride (Si_3N_4)," *Handbook of Optical Constants of Solids*, E. D. Palik (ed.), Academic Press, Orlando (1985), pp. 771-774.

[33] A. H. Clark, "Optical-Properties of Polycrystalline Semiconductor-Films," *Solar Cells*, vol. **1** (1980), pp. 213-215.

[34] G. E. Jellison, M. Keefer, and L. Thornquist, "Spectroscopic Ellipsometry and Interference Reflectometry Measurements of Cvd Silicon Grown on Oxidized Silicon," *Mat. Res. Soc. Symp. Proc.*, vol. **283** (1993), pp. 561-566.

[35] G. Lubberts, B. C. Burkey, F. Moser, and E. A. Trabka, "Optical-Properties of Phosphorus-Doped Polycrystalline Silicon Layers," *J. Appl. Phys.*, vol. **52** (1981), pp. 6870-6878.

[36] Y. J. Cho, N. V. Nguyen, C. A. Richter, J. R. Ehrstein, B. H. Lee, and J. C. Lee, "Spectroscopic Ellipsometry Characterization of High-*k* Dielectric HfO_2 Thin Films and the High-Temperature Annealing Effects on Their Optical Properties," *Appl. Phys. Lett.*, vol. **80** (2002), pp. 1249-1251.

[37] Y. Z. Hu and S. P. Tay, "Characterization of High-K Dielectric ZrO_2 Films Annealed by Rapid Thermal Processing," *J. Vac. Sci. Technol. B*, vol. **19** (2001), pp. 1706-1714.